ROYAL SOCIETY
OF CHEMISTRY

PAPER
Parameswar Krishnan Iyer, Franck Meyer *et al.*
Dual-modal detection of perfluorooctanoic acid (PFOA)
using a single polymer platform: ACQ and IDA approaches

Check for updates

Dual-modal detection of perfluorooctanoic acid (PFOA) using a single polymer platform: ACQ and IDA approaches†

Arvin Sain Tanwar,[a] Parameswar Krishnan Iyer [ID] *[b] and Franck Meyer [ID] *[a]

Perfluorooctanoic acid (PFOA), a prominent member of per- and polyfluoroalkyl substances (PFAS), poses significant environmental and health risks due to its persistence and toxicity. We report a dual-modal sensing strategy employing the water-soluble conjugated polyelectrolyte, poly(3,3'-((1,4-phenylenebis (oxy))bis(propane-3,1-diyl))bis(1-methyl-1*H*-imidazol-3-ium) bromide) (PPMI), for instant detection of PFOA. PPMI exhibits aggregation-caused quenching (ACQ) and indicator displacement assay (IDA) "turn-on" responses towards PFOA in aqueous media. The ACQ mechanism yields a limit of detection (LOD) of 0.21 μM. In contrast, the IDA approach achieves a remarkably lower LOD of 16.1 nM. Notably, PPMI detects PFOA in the presence of potentially interfering ions and distinguishes it from structurally similar PFOA analogues. This dual-modal approach offers a reliable method for PFOA monitoring in environmental water samples.

Introduction

Over the past century, the unique properties of C–F bonds, coupled with the development of innovative fluorination methodologies, have opened new avenues in bio-nanotechnology, as well as in medicinal and materials sciences. Notably, more than 30% of marketed drugs and 50% of blockbuster drugs contain fluorinated molecules.[1,2] In addition fluorine-containing molecules find applications in the medical field, such as ^{19}F MRI contrast agents and therapies like photodynamic, ultrasound, and radiation treatments.[3] The incorporation of fluorine atoms into conjugated polymers allows for the modulation of HOMO–LUMO energy levels, optical properties, film morphology, and charge transport properties, thereby enhancing the performance of organic electronic devices.[4,5] Finally, fluoropolymers are a class of bio-inert, safe compounds with exceptional thermal, chemical, and UV stability, as well as resistance to aging, making them ideal for demanding applications such as high-performance coatings, electronics, transport and medical devices.[6] However, perfluoroalkyl and polyfluoroalkyl substances (PFAS), including perfluorooctanoic

acid (PFOA), are a class of highly persistent organic pollutants that pose significant environmental and health concerns.[7,8] The strong carbon–fluorine bond is the key factor behind their remarkable stability and resistance to natural degradation, making PFAS a significant and enduring environmental challenge.[9,10] These "forever chemicals" are utilized in various industrial applications, including firefighting foams, non-stick cookware, and water-repellent fabrics, contributing to their widespread presence in the environment.[11] Once released into ecosystems, PFAS persist for extended periods and accumulate in water sources, leading to contamination of drinking water supplies and subsequent bioaccumulation in the food chain.[12,13] The adverse health effects associated with long-term PFAS exposure, including cancer, immune system suppression, liver damage, and reproductive disorders, have driven the urgent need for effective detection and remediation strategies to mitigate their impact on public health.[14–16]

Traditional methods for PFOA detection, such as liquid chromatography-mass spectrometry (LC-MS), are widely regarded for its sensitivity and specificity.[17,18] The U.S. Environmental Protection Agency (EPA) has approved several LC-MS protocols, including methods 533, 537, and 1633, which are commonly employed for the analysis of PFAS in environmental samples, particularly drinking water.[19,20] Despite their high accuracy, these techniques present significant practical challenges, including expensive instrumentation, complex sample preparation, time-consuming analysis, and the need for highly trained personnel. The requirements for solid-phase extraction (SPE) in LC-MS methods further

[a]Microbiology, Bioorganic and Macromolecular Chemistry (MBMC) Unit, Faculty of Pharmacy, Université Libre de Bruxelles, 1050 Brussels, Belgium. E-mail: franck.meyer@ulb.be
[b]Department of Chemistry, Indian Institute of Technology Guwahati, Guwahati 781 039, India. E-mail: pki@iitg.ac.in
†Electronic supplementary information (ESI) available: Experimental details, spectroscopy data, *etc.* See DOI: https://doi.org/10.1039/d4lp00344f

© 2025 The Author(s). Published by the Royal Society of Chemistry

RSC Appl. Polym., 2025, **3**, 811–819 | 811

complicate the workflow, making these techniques less feasible for rapid, on-site monitoring of PFAS contamination.[21–23]

To address the limitations of conventional analytical techniques, various alternative methods, such as electrochemical, fluorescence, and colorimetric approaches, among others, have been explored.[24–28] Optical sensing technologies have emerged as promising alternatives for PFAS detection.[29] Fluorescence-based sensors, in particular, have attracted considerable attention due to their inherent advantages, including low cost, portability, fast response times, and the potential for real-time, on-site monitoring.[30–37] These optical sensors exploit fluorescence signals to detect the presence of target analytes, making them especially suitable for environmental applications. However, the development of highly selective fluorescent sensors for PFOA remains a challenge. Many existing sensors suffer from insufficient selectivity, particularly in distinguishing between structurally similar PFAS compounds. Additionally, PFOA itself is non-fluorescent, necessitating the use of indirect detection methods, such as fluorescence quenching or signal enhancement through probe interactions. These approaches, while effective, often complicate the detection process and may compromise selectivity.

In recent years, conjugated polymer-based sensors have demonstrated tremendous potential for improving sensitivity and selectivity in PFAS detection.[31,32,37] Conjugated polymers, with their extended π-conjugation and delocalized electronic structures, exhibit excellent light-harvesting properties and signal amplification capabilities, which make them ideal candidates for the development of sensitive optical sensors and thus have been explored for various metal ions, anions, explosives, chemo-sensing and bio-sensing applications.[38–42] In this study, we present a novel sensing platform based on the conjugated polyelectrolyte poly(3,3′-((1,4-phenylenebis(oxy))bis(propane-3,1-diyl))bis(1-methyl-1H-imidazol-3-ium) bromide) (PPMI), combined with uranine dye (UD), for detecting PFOA. Unlike most PFAS-based sensors, this compound was chosen for its low cost, ease of preparation, and excellent optical properties. Its affordability and superior optical performance make it an ideal candidate for routine experimental use. This system operates via an indicator displacement assay (IDA) mechanism, where the displacement of the dye upon interaction with PFOA triggers a measurable fluorescence response.[30,43] The PPMI-UD system demonstrates a sensitive, selective and instant response to PFOA in aqueous medium, overcoming the limitations of previously reported optical sensors (Table 1).

To the best of our knowledge, this is the first demonstration of a dual-mode sensing platform that employs both fluorescence "turn-off" and "turn-on" mechanisms for the selective detection of PFOA in aqueous environments. The PPMI-UD system effectively distinguishes PFOA from other PFAS compounds, offering real-time, on-site detection approach with excellent sensitivity at pH 7.2. This study provides a significant advancement in the field of PFAS detection, particularly for environmental monitoring, where rapid and selective detection methods are critically needed.

Table 1 Comparison of some recent fluorescence-based sensing materials developed for PFOA detection

Material used	Detection limit	Concentration range	Medium used	Sensing approach	Ref.
Water-soluble conjugated polyelectrolyte	0.21 μM (ACQ) and 16.1 nM (6.67 ppb) (IDA)	0–40 μM	H$_2$O (HEPES, pH 7.2)	ACQ (turn OFF) and IDA (turn ON)	This work
Guanidinocalix[5]arene	26.4 nM (10.9 μg L^{-1})	0–2484 ppb	HEPES buffer [pH 7.4]	IDA (turn ON)	30
PDI based MOF	1.68 μM (in aqueous suspension) & 3.1 nM (onto paper)	0–20 μM	H$_2$O : DMF (60 : 40, v/v)	Fluorescence turn ON	34
Conjugated polymer films and CPdots	1 ppb (2.4 nM) and 0.08 ppb (0.2 nM) (incubation time = 1 h)	0–50 ppb and 0–5 ppb (incubation time = 1 h)	Water	Ratiometric	32
Conjugated polymer/dye combinations	126 ppb–59 ppb	0–1000 ppb	Water	Ratiometric	33
Conjugated polymer	6.12 nM	0–20 μM	DMSO/HEPES buffer (pH 7.2)	Ratiometric	31
AIEgen	41 ppb	0.1–100 μM; 41–41 000 ppb	Organic solvents	Fluorescence turn ON	45
Erythrosin B-CTAB system	4.9 ppb (11.8 nM)	21–4141 ppb	Britton–Robinson (BR) buffer (pH 8.5)	Fluorescence turn ON	46
Se and N doped-carbon dot	745.2 ppb (1.8 μM)	4141–28 985 ppb (10 to 70 μM)	pH 8.0	Fluorescence turn OFF	35
Water-soluble CdS quantum dots (QDs)	0.3 μM	0.5–40 μM	pH 10.0	Fluorescence turn OFF	36
Quantum dots (QDs) coated with molecularly imprinted polymer (MIP)	25 nM (~10 ppb)	0.25–15.00 μM	NaAc–HAc buffer, pH 3.8.	Fluorescence turn OFF	47

Experimental section

Materials and methods

Perfluorooctanoic acid (PFOA) and 4-(2-hydroxyethyl)piperazine-1-ethanesulfonic acid (HEPES) and trifluoroacetic acid (TFA) were purchased from Sigma-Aldrich. Octanoic acid (OA) was obtained from BLD Pharmatech GmbH. Butyric acid (BA) was purchased from Carl Roth GmbH. Heptafluorobutyric acid (HFBA) was purchased from Apollo Scientific. Uranine dye (UD) was obtained from Tokyo Chemical Industry (TCI). All other electrolyte salts (sodium chloride, calcium chloride, potassium chloride, sodium hydrogen carbonate, potassium carbonate, sodium acetate, sodium sulfate *etc.*) were received from various chemical companies such as VWR chemical, Chem-Lab NV, Merck *etc.* MilliQ-water was used as solvent media for all the fluorescence and absorbance studies. Fluorescence spectra were recorded from fluoromax-4 spectrofluorometer. Absorbance spectra were recorded from UV-1800 Shimadzu UV spectrophotometer. Quartz cuvettes with a 10 mm path length were used in fluorescence and absorbance studies. A 1 mM stock solution of all the analytes was prepared in water and further diluted whenever required in the study. For ACQ approach, the fluorescence and absorbance studies of PPMI were conducted in aqueous media buffered with 10 mM HEPES (pH 7.2) in the presence of varying PFOA concentrations (0–100 μM). Furthermore, for IDA approach, the fluorescence and absorbance studies of UD were performed in aqueous media buffered with 10 mM HEPES (pH 7.2) at different PPMI concentrations (0–40 μM). All solutions were thoroughly mixed at room temperature prior to analysis and the concentration of UD was kept constant during the analysis. Dynamic light scattering (DLS) was measured using a Malvern Zetasizer.

Synthesis of poly(3,3′-((1,4-phenylenebis(oxy))bis(propane-3,1-diyl))bis(1-methyl-1*H*-imidazol-3-ium) bromide) (PPMI)

The conjugated polyelectrolyte PPMI was synthesized according to our previously established method.[44] The precursor polymer PPBr (18 mg) was dissolved in dimethylformamide (DMF) in a round-bottom flask, followed by the addition of 1-methylimidazole (82 μL). The reaction mixture was stirred for 24 hours at 70 °C under an argon atmosphere. Subsequently, the mixture was precipitated into diethyl ether. The resulting precipitate was washed multiple times with chloroform to remove residual reactants. Finally, a brown-colored, sticky PPMI polymer was obtained with a yield of 70%. ^{1}H NMR (400 MHz, D$_2$O, δ): 8.47 (b), 7.45 (b), 7.40 (b), 7.20 (b), 4.20 (b), 3.91 (b), 3.87(b), 2.25(b).

LOD calculations

To determine the detection limit for the ACQ approach, solutions of the polymer PPMI (0.33 μM) spiked with varying concentrations of PFOA (0, 0.66, 1.33, 2.0, 2.66, and 3.33 μM) were prepared in 10 mM HEPES buffer (pH 7.2). Emission spectra were recorded for each sample upon excitation at 318 nm. A calibration curve was constructed by plotting fluorescence intensity against PFOA concentration, yielding a linear regression equation. The limit of detection (LOD) was calculated using the $3\sigma/k$ criterion, where σ represents the standard deviation of PPMI's fluorescence intensity in the absence of PFOA and k is the slope of the calibration curve, which reflects the sensitivity of the detection system. The reasoning is based on the signal-to-noise ratio: a detectable signal should be at least three times greater than the noise level to ensure reliability. Thus, dividing $3 \times \sigma$ by the slope (k) gives the analyte concentration at which the signal is distinguishable from the noise.[31,34]

To determine the detection limit for the IDA approach, solutions of PPMI (80 nM) and UD (0.1 μM) spiked with PFOA (0, 0.66, 1.33, 2.0, 2.66, and 3.33 μM) were prepared in 10 mM HEPES buffer (pH 7.2). Fluorescence spectra were recorded for each sample at λ_{ex} = 490 nm. Calibration plots of fluorescence intensity *vs.* PFOA concentration yielded linear regression equations (R^2 > 0.99). The limit of detection (LOD) was calculated using the $3\sigma/k$ criterion, where σ is the standard deviation of fluorescence intensity for UD and PPMI in the absence of PFOA, and k is the slope of the calibration curve.
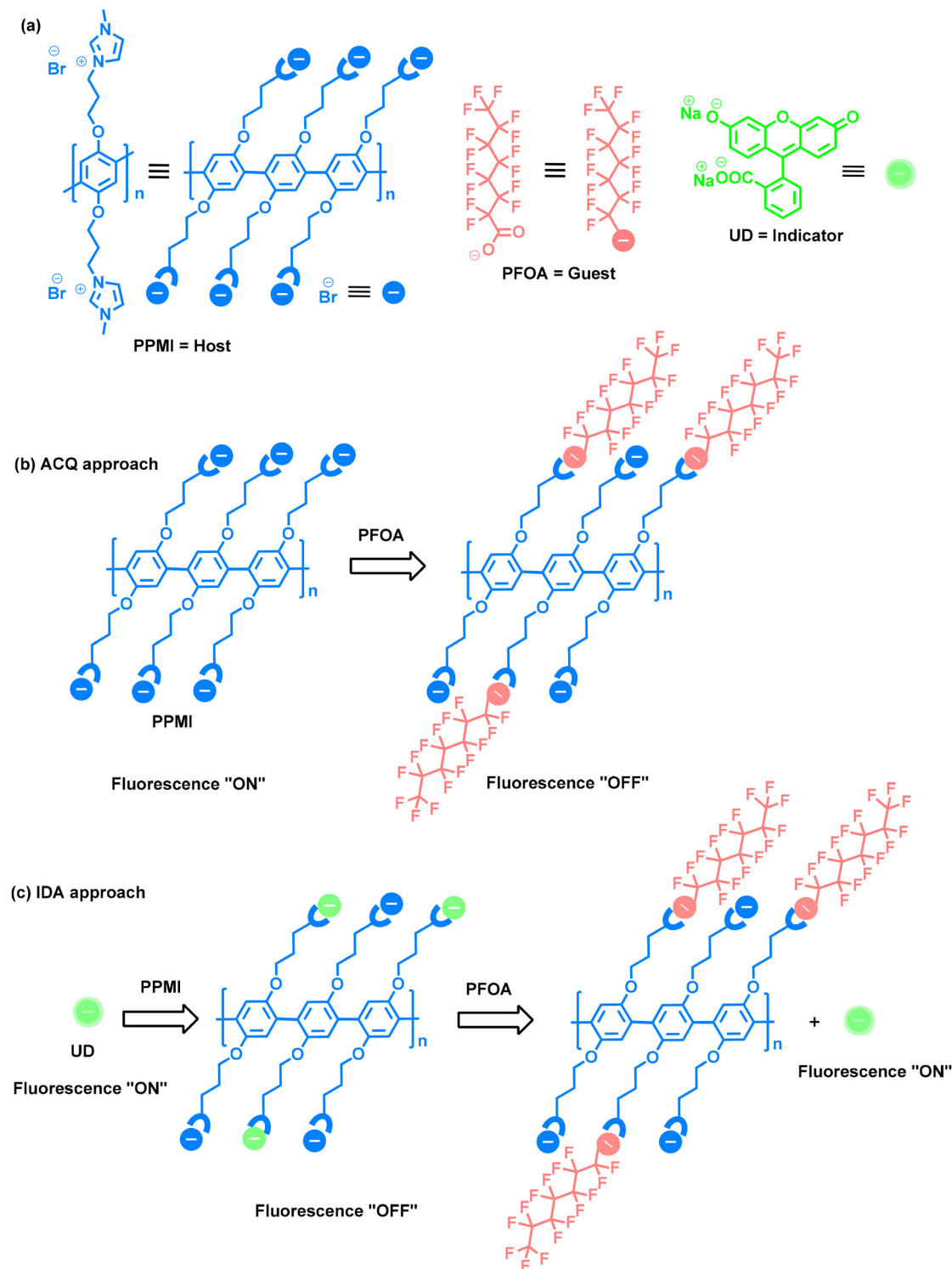
Results and discussion

Scheme 1 presents the chemical structure of PPMI, a polyelectrolyte sharing architectural features with ionic conjugated polymers and conjugated polyelectrolytes. PPMI was synthesized through the polymerization of 1,4-bis(3-bromopropoxy)benzene with anhydrous iron chloride, followed by quaternization with methylimidazole, following a previously reported method.[44,48,49] The cationic imidazolium terminals on PPMI's side chains enhance its solubility in polar solvents, such as water, and facilitate ionic attraction with anionic species, such as PFOA, through ion exchange. The resulting cationic polyelectrolyte exhibits strong fluorescence in water, characterized by a photoluminescence (PL) quantum yield of 0.23. The two different sensing approaches such as ACQ and IDA were performed in aqueous solutions buffered with 10 mM HEPES (pH 7.2) and the results are discussed.

Sensing studies using ACQ method

To evaluate the sensing performance of PPMI towards PFOA, fluorescence titrations were conducted by gradually increasing the concentration of PFOA (0–100 μM) in an aqueous solution containing highly fluorescent PPMI (0.33 μM) (Fig. 1a). Upon the initial addition of a 16.6 μM of PFOA, a rapid reduction of approximately 20% in the PL intensity of PPMI was observed. As the concentration of PFOA continued to increase, the PL intensity decreased further, achieving a quenching efficiency of around 89% (Fig. 1a). This behaviour indicates that PPMI is sensitive to PFOA. Along with the PPMI emission peak, another peak around 356 nm was observed which corresponds to the Raman scattering of water (excitation = 318 nm). To further investigate the quenching efficiency, a Stern–Volmer plot was generated to determine the Stern–Volmer constant (K_{sv}) (Fig. 1b). The plot displayed a linear relationship at lower

© 2025 The Author(s). Published by the Royal Society of Chemistry

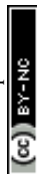*RSC Appl. Polym.*, 2025, **3**, 811–819 | 813

Scheme 1 (a) Chemical structure of the components: polymeric host (PPMI), guest (perfluorinated pollutant, PFOA) and fluorescent indicator (uranine dye, UD). Illustration of (b) ACQ and (c) IDA sensing approaches.

PFOA concentrations.[50] However, at higher concentrations, the plot deviated from linearity, implying the presence of mixed quenching processes such as aggregation or the inner-filter effect, alongside possible static and dynamic quenching

(Fig. 1b).[41,51] The LOD for the ACQ method was calculated to be 0.21 μM (Fig. 1c). Moreover, the absorption spectra of PPMI (0.33 μM) at varying concentrations of PFOA (0–100 μM) (Fig. 1d) exhibited a noticeable shift, with a new absorption
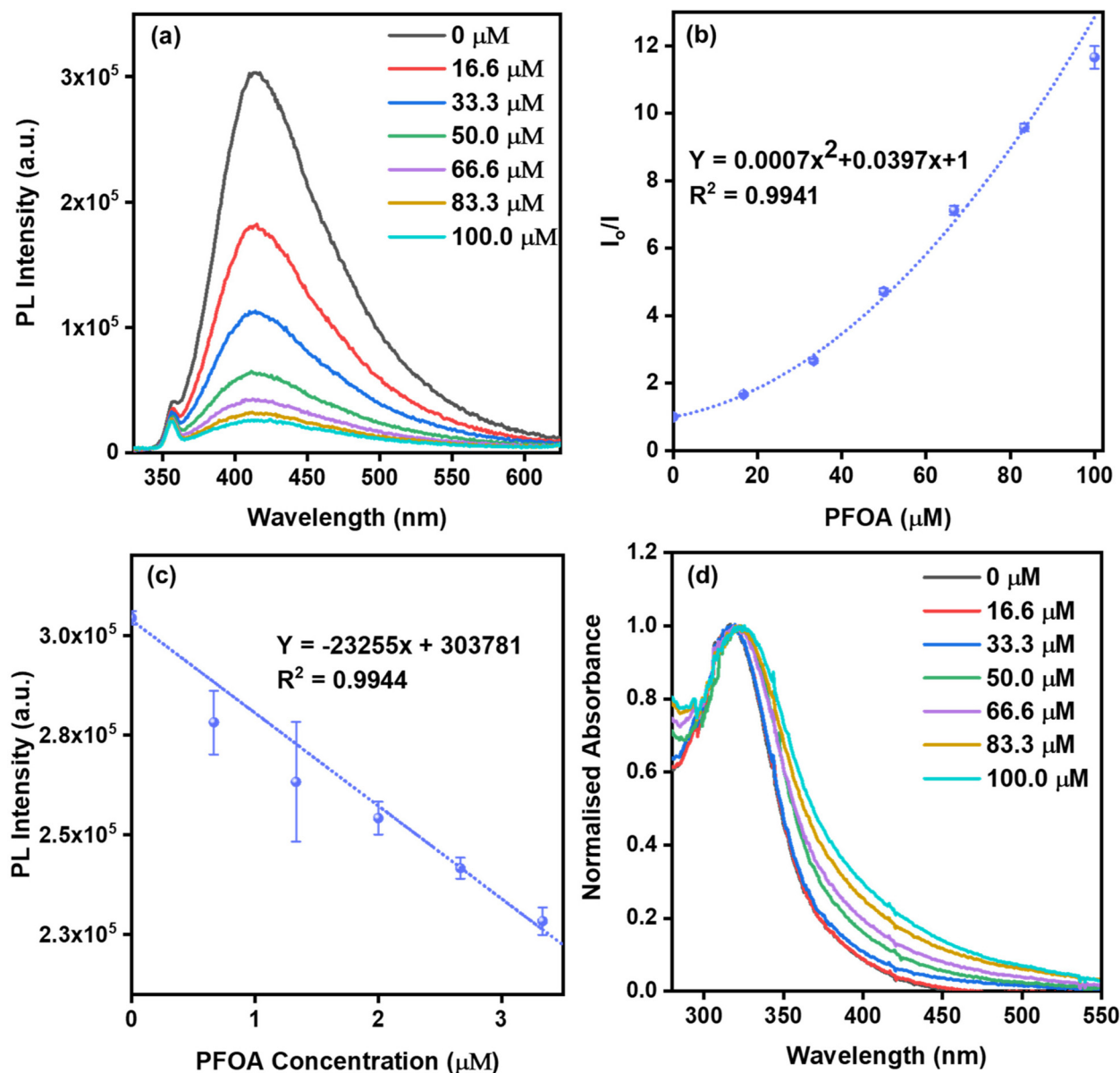
Fig. 1 Sensing studies performed with ACQ approach: (a) fluorescence spectra of PPMI (0.33 μM) with respect to change in the PFOA concentration in HEPES buffer (10 mM, pH 7.2) (excitation wavelength = 318 nm, slit width = 2 nm). (b) Stern–Volmer plots for PFOA detection, illustrating the quenching efficiency. (c) LOD plot for PFOA, showcasing sensitivity. (d) Normalized absorbance spectra of PPMI (0.33 μM) at varying PFOA concentrations in HEPES buffer (10 mM, pH 7.2).

band appearing around 425 nm. This shift suggests the formation of electrostatic complexes and aggregation of PPMI as a result of PFOA binding. Further, we conducted DLS studies with PPMI dissolved in HEPES buffer (10 mM, pH 7.2) but no significant readings were obtained. This indicates that the highly water-soluble nature of ionic PPMI prevents notable light scattering. However, upon the addition of negatively charged PFOA, we observed significant light scattering, indicating the formation of nanoaggregates with a diameter of approximately 200 nm (Fig. S5†). These findings strongly suggest that PPMI forms electrostatic complexes with PFOA, leading to nanoaggregate formation.

Sensing studies using the IDA method

In a typical indicator displacement assay (IDA) sensing system, three key components are involved: (1) an indicator (dye) that generates the sensing signal, (2) a host that accommodates the indicator, and (3) a target analyte that displaces the indicator from the host. In this study, uranine dye (UD), a sodium salt of fluorescein, was employed as the indicator dye (Scheme 1). UD exhibits absorption and fluorescence maxima at 490 nm and 513 nm, respectively, with excitation at 490 nm in HEPES-buffered water (pH 7.2, 10 mM). For all titration experiments, the concentration of UD was maintained at 0.1 μM. In prelimi-
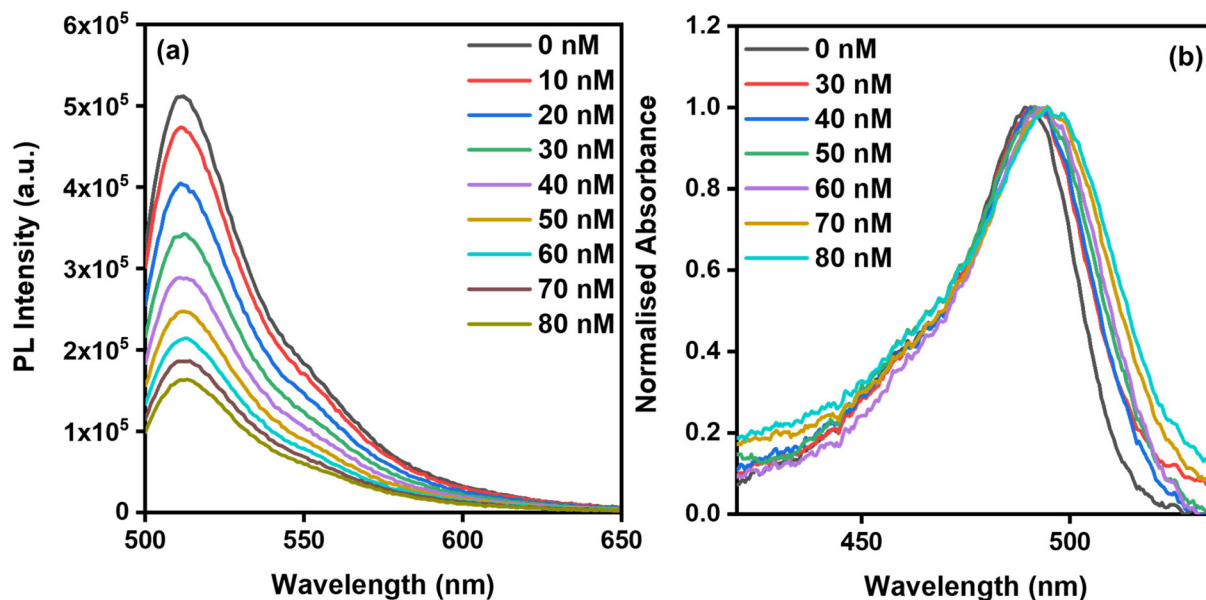
© 2025 The Author(s). Published by the Royal Society of Chemistry

RSC Appl. Polym., 2025, **3**, 811–819 | **815**

Fig. 2 (a) Fluorescence spectra and (b) normalized absorbance spectra of UD (0.1 μM) with increasing PPMI concentration in HEPES buffer (10 mM, pH 7.2) (excitation wavelength = 490 nm, slit width = 2 nm).

nary experiments, the fluorescence of UD (0.1 μM) in HEPES-buffered water (pH 7.2, 10 mM) was measured in the presence of increasing concentrations of PPMI (0–80 nM) (Fig. 2a). The fluorescence intensity of UD gradually decreased with the addition of PPMI, showing a 63% quenching after the addition of 80 nM of PPMI. Additionally, the absorbance spectra of UD were analyzed after the addition of varying concentrations of PPMI (0–80 nM) (Fig. 2b). The absorbance maximum of UD, initially at 490 nm, exhibited a red shift of 5 nm, moving to 495 nm. This new peak at 495 nm in the absorbance spectrum signifies the formation of a host/dye complex, specifically the PPMI/UD complex.

To investigate the displacement of UD from the cationic conjugated polymer PPMI by PFOA, IDA studies were performed using quartz cuvettes. The concentration of the PPMI (80 nM)/UD (0.1 μM) complex was kept constant in HEPES-buffered water (pH 7.2, 10 mM), while the concentration of PFOA was varied from 0 to 40 μM. In these experiments, the fluorescence spectra of the PPMI/UD complex were recorded at different concentrations of PFOA (0–40 μM) (Fig. 3a). As the concentration of PFOA increased, a gradual enhancement in fluorescence intensity was observed, leading to a reversible dequenching effect upon the addition of 40 μM of PFOA. A plot of PL intensity *versus* PFOA concentration revealed saturation of the curve around 40 μM (Fig. S8†). Additionally, a plot of I/I_0 *versus* PFOA concentration demonstrated a second-order relationship, with a fitting R^2 value of 0.9940 (Fig. S9†). Additionally, the absorption spectra of the PPMI/UD complex were recorded under similar conditions with increasing concentrations of PFOA (Fig. 3b). Initially, the absorbance maximum of the PPMI/UD complex was observed at 495 nm. However, as the concentration of PFOA increased, this absor-

bance maximum blue-shifted back to 490 nm, indicating that UD was being displaced from the PPMI/UD complex upon interaction with PFOA (Scheme 1c).

The limit of detection (LOD) was assessed by monitoring changes in the emission spectrum of the PPMI (80 nM)/UD (0.1 μM) complex at various concentrations of PFOA (0.66 μM, 1.33 μM, 2.0 μM, 2.66 μM, 3.33 μM). The LOD, calculated using the equation $3\sigma/K$, was determined to be 16.1 nM (6.67 ppb) (Fig. S1†), which is comparable to other reported PFOA sensors developed for optical detection in any solution (Table 1).

Smartphone-assisted real-time monitoring

A photograph of the PPMI (80 nM)/UD (0.1 μM) complex solution in HEPES buffer (pH 7.2, 10 mM) was captured under UV light (365 nm) after successive additions of PFOA (0–36.6 μM) using a Samsung S23 Ultra smartphone (Fig. 4a). Both the emission of unbound PPMI and Raman scattering fall within the blue fluorescence region when the PPMI and UD solution is excited at 365 nm (Fig. S6†). As the PFOA concentration increases, the green channel fluorescence intensifies due to dye displacement, while the blue emission from unbound PPMI is quenched. Consequently, the ratio of green to blue fluorescence was selected as a more representative metric for the sensing mechanism. The colour intensity (RGB values) of each cuvette was analysed using a Colour Picker application, and the G/B ratio was plotted against the PFOA concentration (Fig. 4b). A linear fit was observed, demonstrating the effectiveness of the IDA method for real-time sensing and quantification of PFOA.

Selectivity studies

To assess the selectivity of the sensor, fluorescence-based IDA experiments were conducted by adding various common PFOA

816 | *RSC Appl. Polym.*, 2025, **3**, 811–819

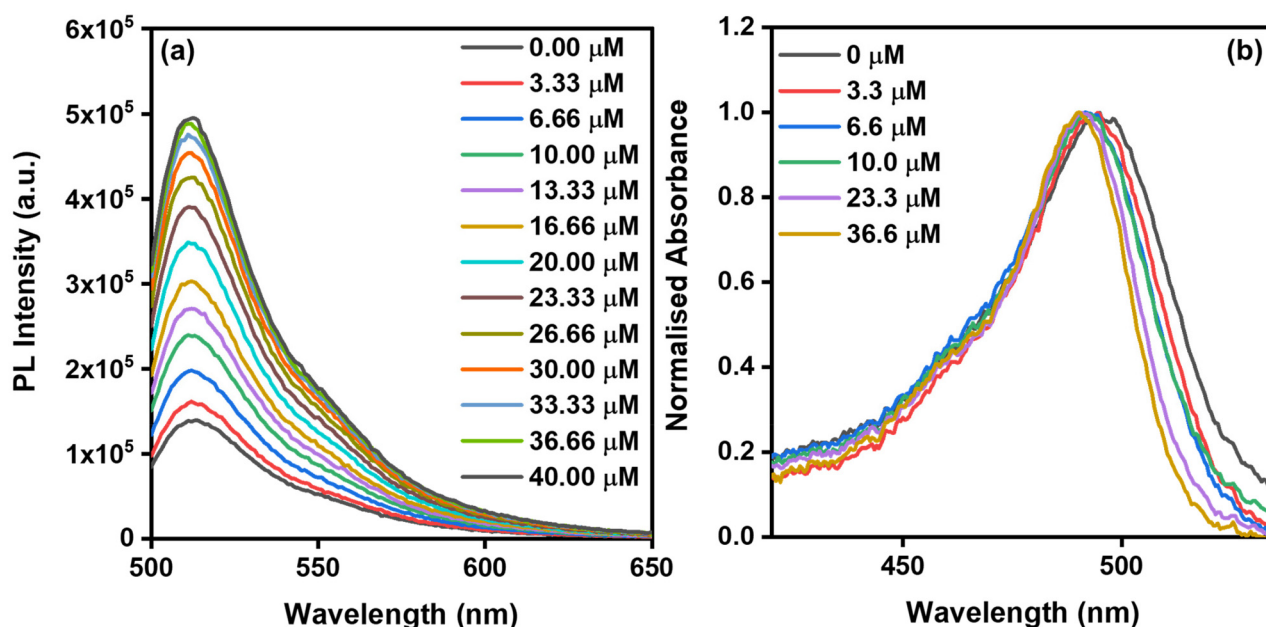© 2025 The Author(s). Published by the Royal Society of Chemistry

Fig. 3 (a) Fluorescence spectra and (b) normalized absorbance spectra of UD (0.1 µM)/PPMI (80 nM) complex with increasing PFOA concentrations in HEPES buffer (10 mM, pH 7.2) (excitation wavelength = 490 nm, slit width = 2 nm).
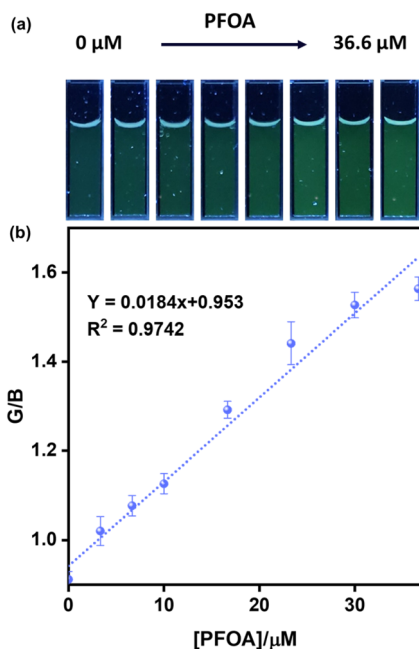

Fig. 4 Smartphone-assisted real-time monitoring of PFOA. (a) Images of UD (0.1 µM)/PPMI (80 nM) complex solution under UV irradiating lamp (365 nm) with varying PFOA concentrations captured *via* Samsung S23 Ultra smartphone. (b) G/B colour intensity ratios *vs.* PFOA concentrations in HEPES buffer (10 mM, pH 7.2), extracted using Colour Picker application.
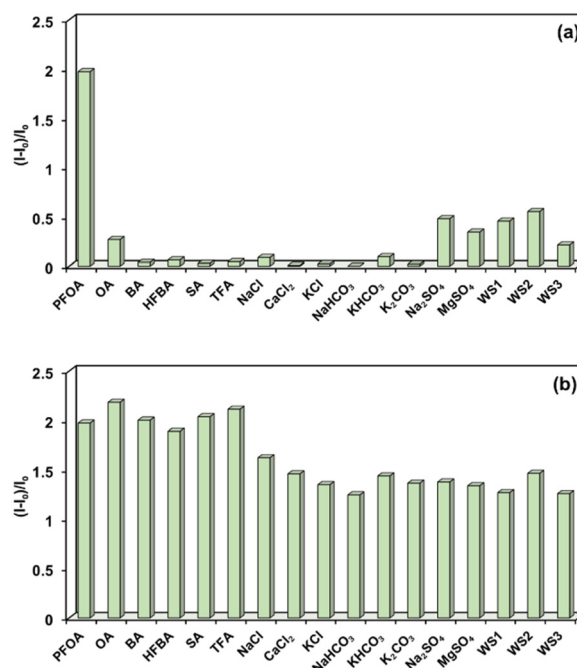

Fig. 5 Fluorescence responses of UD (0.1 µM)/PPMI (80 nM) complex towards various PFAS analogues (40 µM), common waterborne interfering ions and different water samples (a) in absence and (b) in presence of PFOA (40 µM) (excitation wavelength = 490 nm, slit width = 2 nm).

analogs (Fig. S10†), including octanoic acid (OA), butyric acid (BA), heptafluorobutyric acid (HFBA), sodium acetate (SA), and trifluoroacetic acid (TFA), as well as common electrolyte salts such as NaCl, CaCl$_2$, KCl, NaHCO$_3$, KHCO$_3$, K$_2$CO$_3$, Na$_2$SO$_4$, and MgSO$_4$ to the PPMI (80 nM)/UD (0.1 µM) complex in HEPES-buffered water (pH 7.2, 10 mM) (Fig. 5a, S2 and S3†). Remarkably, the addition of these analytes resulted in no sig-

nificant changes in the fluorescence spectra of the PPMI/UD complex. Additionally, natural water samples, including WS1 (tap water), WS2 (drinking tap water), and WS3 (ground water), showed no notable effect on the fluorescence of the PPMI/UD complex (Fig. 5a, and S4†), confirming the sensor's selectivity for PFOA in IDA studies. To further evaluate performance in a competitive environment, sensing experiments were performed by first adding OA (40 μM) to the PPMI (80 nM)/UD (0.1 μM) complex in buffered water. No significant change in emission intensity was observed (Fig. S3†). However, upon subsequent addition of PFOA (40 μM), a substantial fluorescence enhancement was recorded. This procedure was repeated with other PFAS analogs and electrolyte salts, yielding similar fluorescence "turn-on" responses following PFOA addition (Fig. S2 and S3†). It is worth mentioning that most existing chemosensor systems for PFOA detection operate on either a turn-off or turn-on mechanism, whereas the present sensing system offers two methods based on a single polymeric platform. Studies involving polymers for sensing PFOA analogs have demonstrated similar selectivity while proposing various mechanisms, including protonation, polymer aggregation, fluorous phase accumulation driven by perfluorochains, and ion-exchange processes.[31–33] In a small host–guest system with PFOA, some researchers successfully obtained single-crystal data, revealing the orientation of interactions between imidazolium-based receptors and PFOA.[52] Based on the available evidence, it can be concluded that selectivity in this system is primarily governed by ion-exchange processes, facilitated by fluorous phase interactions arising from the perfluorochains of PFOA. Overall, the IDA based approach stands out as a sensitive, simple, rapid, and reliable method for detecting PFOA, even in competitive environments and drinking water samples.

Conclusions

In this study, we developed a dual-modal sensing platform based on a cost-effective and easily synthesized conjugated polyelectrolyte poly(3,3′-((1,4-phenylenebis(oxy))bis(propane-3,1-diyl))bis(1-methyl-1H-imidazol-3-ium) bromide) (PPMI) for the selective detection of PFOA in aqueous environments. The platform combines aggregation-caused quenching (ACQ) and indicator displacement assay (IDA) mechanisms, achieving detection limits of 0.21 μM and 16.1 nM, respectively, with the IDA approach demonstrating superior sensitivity. The sensor exhibited selective behavior for PFOA in the presence of structurally similar PFOA analogues and common electrolytes, highlighting its effectiveness for environmental monitoring. Furthermore, the sensor's real-time detection capability was demonstrated using smartphone-assisted analysis. This dual-modal system represents the first instance of a single polymeric platform capable of both "turn-off" and "turn-on" sensing for PFOA, providing a simple, rapid, and reliable approach for real-world environmental applications. Overall, the ease of synthesis and low cost of PPMI makes it a promis-

ing alternative to other sensing materials reported in the literature.

Data availability

The data supporting this article have been included as part of the ESI.†

Conflicts of interest

There are no conflicts to declare.

Acknowledgements

References

1 S. Ali and J. Zhou, *Eur. J. Med. Chem.*, 2023, **256**, 115476.
2 F. Meyer, *Chem. Commun.*, 2016, **52**, 3077–3094.
3 C. Zhang, K. Yan, C. Fu, H. Peng, C. J. Hawker and A. K. Whittaker, *Chem. Rev.*, 2022, **122**, 167–208.
4 T. Zhang, Z. Chen, W. Zhang, L. Wang and G. Yu, *Adv. Mater.*, 2024, **36**, 1–30.
5 F. Meyer, *Prog. Polym. Sci.*, 2015, **47**, 70–91.
6 B. Ameduri, *J. Fluor. Chem.*, 2023, **267**, 110117.
7 S. Y. Wee and A. Z. Aris, *npj Clean Water*, 2023, **6**, 57.
8 R. C. Buck, J. Franklin, U. Berger, J. M. Conder, I. T. Cousins, P. de Voogt, A. A. Jensen, K. Kannan, S. A. Mabury and S. P. J. van Leeuwen, *Integr. Environ. Assess. Manage.*, 2011, **7**, 513–541.
9 D. O'Hagan, *Chem. Soc. Rev.*, 2008, **37**, 308–319.
10 M. K. Wilsey, T. Taseska, Z. Meng, W. Yu and A. M. Müller, *Chem. Commun.*, 2023, **59**, 11895–11922.
11 D. Herzke, E. Olsson and S. Posner, *Chemosphere*, 2012, **88**, 980–987.
12 J. M. Graber, C. Alexander, R. J. Laumbach, K. Black, P. O. Strickland, P. G. Georgopoulos, E. G. Marshall, D. G. Shendell, D. Alderson, Z. Mi, M. Mascari and C. P. Weisel, *J. Exposure Sci. Environ. Epidemiol.*, 2019, **29**, 172–182.
13 F. Suja, B. K. Pramanik and S. M. Zain, *Water Sci. Technol.*, 2009, **60**, 1533–1544.
14 B. Vaughn, W. Andrea and S. Kyle, *Environ. Health Perspect.*, 2013, **121**, 1313–1318.

15 E. M. Sunderland, X. C. Hu, C. Dassuncao, A. K. Tokranov, C. C. Wagner and J. G. Allen, *J. Exposure Sci. Environ. Epidemiol.*, 2019, **29**, 131–147.

16 E. M. Bell, S. De Guise, J. R. McCutcheon, Y. Lei, M. Levin, B. Li, J. F. Rusling, D. A. Lawrence, J. M. Cavallari, C. O'Connell, B. Javidi, X. Wang and H. Ryu, *Sci. Total Environ.*, 2021, **780**, 146399.

17 E. Piva, P. Fais, G. Cecchetto, M. Montisci, G. Viel and J. P. Pascali, *J. Chromatogr. B: Anal. Technol. Biomed. Life Sci.*, 2021, **1172**, 122651.

18 J. P. Benskin, M. Bataineh and J. W. Martin, *Anal. Chem.*, 2007, **79**, 6455–6464.

19 EPA PFAS Drinking Water Laboratory Methods. https://www.epa.gov/pfas/epa-pfas-drinking-water-laboratory-methods, (accessed 14 October 2024).

20 Epa, Ow and Ost, Method 1633 Analysis of Per- and Polyfluoroalkyl Substances (PFAS) in Aqueous, Solid, Biosolids, and Tissue Samples by LC-MS/MS. https://www.epa.gov (accessed October 14, 2024).

21 J. N. Dodds, N. L. M. Alexander, K. I. Kirkwood, M. R. Foster, Z. R. Hopkins, D. R. U. Knappe and E. S. Baker, *Anal. Chem.*, 2021, **93**, 641–656.

22 H. Ryu, B. Li, S. De Guise, J. McCutcheon and Y. Lei, *J. Hazard. Mater.*, 2021, **408**, 124437.

23 J. Kidd, E. Fabricatore and D. Jackson, *Sci. Total Environ.*, 2022, **836**, 155523.

24 R. B. Clark and J. E. Dick, *Chem. Commun.*, 2021, **57**, 8121–8130.

25 A. Tasfaout, F. Ibrahim, A. Morrin, H. Brisset, I. Sorrentino, C. Nanteuil, G. Laffite, I. A. Nicholls, F. Regan and C. Branger, *Talanta*, 2023, **258**, 124434.

26 R. F. Menger, E. Funk, C. S. Henry and T. Borch, *Chem. Eng. J.*, 2021, **417**, 129133.

27 T. Y. Guo, H. W. Li, C. X. Zhang and Y. Wu, *Analyst*, 2023, **148**, 3931–3937.

28 C. M. Taylor, M. C. Breadmore and N. L. Kilah, *Sens. Diagn.*, 2023, **2**, 676–686.

29 D. Thompson, N. Zolfigol, Z. Xia and Y. Lei, *Sens. Actuators Rep.*, 2024, **7**, 100189.

30 Z. Zheng, H. Yu, W.-C. Geng, X.-Y. Hu, Y.-Y. Wang, Z. Li, Y. Wang and D.-S. Guo, *Nat. Commun.*, 2019, **10**, 5762.

31 X. Chen, S. Hussain, Y. Tang, X. Chen, S. Zhang, Y. Wang, P. Zhang, R. Gao, S. Wang and Y. Hao, *Sci. Total Environ.*, 2023, **860**, 160467.

32 A. Concellón, J. Castro-Esteban and T. M. Swager, *J. Am. Chem. Soc.*, 2023, **145**, 11420–11430.

33 A. Concellón and T. M. Swager, *Angew. Chem., Int. Ed.*, 2023, **62**, e202309928.

34 R. Dalapati, M. Hunter, M. Sk, X. Yang and L. Zang, *ACS Appl. Mater. Interfaces*, 2024, **16**, 32344–32356.

35 L. S. Walekar, M. Zheng, L. Zheng and M. Long, *Microchim. Acta*, 2019, **186**, 278.

36 Q. Liu, A. Huang, N. Wang, G. Zheng and L. Zhu, *J. Lumin.*, 2015, **161**, 374–381.

37 E. E. Harrison and M. L. Waters, *Chem. Sci.*, 2023, **14**, 928–936.

38 A. H. Malik, S. Hussain, A. S. Tanwar, S. Layek, V. Trivedi and P. K. Iyer, *Analyst*, 2015, **140**, 4388–4392.

39 A. S. Tanwar, M. A. Chanu, R. Parui, D. Barman, Y.-H. Im and P. Krishnan Iyer, *RSC Appl. Polym.*, 2024, **2**, 196–204.

40 A. S. Tanwar, R. Parui, R. Garai, M. A. Chanu and P. K. Iyer, *ACS Meas. Sci. Au*, 2022, **2**, 23–30.

41 A. S. Tanwar, L. R. Adil, M. A. Afroz and P. K. Iyer, *ACS Sens.*, 2018, **3**, 1451–1461.

42 M. A. Chanu, S. Mondal, N. Zehra, A. S. Tanwar and P. K. Iyer, *ACS Appl. Polym. Mater.*, 2022, **4**, 3491–3497.

43 A. S. Tanwar and P. K. Iyer, *ACS Omega*, 2017, **2**, 4424–4430.

44 A. S. Tanwar, M. N. Khatun, M. A. Chanu, T. Sarmah, Y. H. Im and P. K. Iyer, *Analyst*, 2023, **148**, 6011–6019.

45 C. Fang, J. Wu, Z. Sobhani, M. Al Amin and Y. Tang, *Anal. Methods*, 2019, **11**, 163–170.

46 Z. Cheng, L. Du, P. Zhu, Q. Chen and K. Tan, *Spectrochim. Acta, Part A*, 2018, **201**, 281–287.

47 L. Zheng, Y. Zheng, Y. Liu, S. Long, L. Du, J. Liang, C. Huang, M. T. Swihart and K. Tan, *Talanta*, 2019, **194**, 1–6.

48 F. Meyer, J.-M. Raquez, O. Coulembier, J. De Winter, P. Gerbaux and P. Dubois, *Chem. Commun.*, 2010, **46**, 5527–5529.

49 E. Manfredi, F. Meyer, P. Verge, J.-M. Raquez, J.-M. Thomassin, M. Alexandre, B. Dervaux, F. Duprez, P. Van Der Voort, C. Jérôme and P. Dubois, *J. Mater. Chem.*, 2011, **21**, 16190–16196.

50 A. S. Tanwar, N. Meher, L. R. Adil and P. K. Iyer, *Analyst*, 2020, **145**, 4753–4767.

51 A. S. Tanwar, S. Hussain, A. H. Malik, M. A. Afroz and P. K. Iyer, *ACS Sens.*, 2016, **1**, 1070–1077.

52 T.-N. Gao, S. Huang, R. Nooijen, Y. Zhu, G. Kociok-Köhn, T. Stuerzer, G. Li, J. H. Bitter, G. I. J. Salentijn, B. Chen, F. M. Miloserdov and H. Zuilhof, *Angew. Chem., Int. Ed.*, 2024, **63**, e202403474.

© 2025 The Author(s). Published by the Royal Society of Chemistry

RSC Appl. Polym., 2025, **3**, 811–819 | 819